Heliyon

Received:
3 November 2018
Revised:
2 January 2019
Accepted:
6 February 2019

Cite as: Ghazala Nazeer, Shams-Ul Islam, Sehrish Hassan Shigri. Numerical investigation of vortex shedding mechanism for staggered rows of cylinders. Heliyon 5 (2019) e01224. doi: 10.1016/j.heliyon.2019.e01224

Numerical investigation of vortex shedding mechanism for staggered rows of cylinders

Ghazala Nazeer [a,*], **Shams-Ul Islam** [b], **Sehrish Hassan Shigri** [c]

[a] *Cholistan University of Veterinary and Animal Sciences, Bahawalpur 63100, Pakistan*

[b] *COMSATS University Islamabad, 44000, Pakistan*

[c] *National University of Computer and Emerging Sciences Islamabad, 44000, Pakistan*

[*] Corresponding author.

E-mail address: ghazala.nazeer@yahoo.com (G. Nazeer).

Abstract

This numerical investigation deals with study of flow past seven square cylinders arranged in staggered configuration. Simulations to the underlying problem are carried out by using the single relaxation time lattice Boltzmann method. The gap spacing between the staggered rows is varied in streamwise direction from 0.25 to 2 and for three transverse spacing i.e. T* = 1, 1.5 and 2. The complex vortex shedding mechanism is visualized for different streamwise and transverse gap spacings. Furthermore, the vortex shedding mechanisms in the wake of downstream row of cylinders are debated by using vorticity snapshots, time-trace plots of drag and lift coefficients and power spectra visualization of lift coefficient. It is also observed that the secondary cylinder interaction frequency contributes significantly to the hydrodynamic forces experienced by the cylinders. The physical parameters, such as Strouhal number, the drag and lift coefficients and their root-mean-square values have also been discussed in detail.

Keyword: Mechanical engineering

1. Introduction

Flows around multiple square cylinders represent an ideal scenario of airflows around buildings which have practical engineering importance and scientific

https://doi.org/10.1016/j.heliyon.2019.e01224

relevance in the field of fluid mechanics and dynamics. Flows experienced around multiple buildings vary from low Reynolds number ($Re = U_\infty d/v$, where U_∞ represents uniform inflow velocity, d is the size of object and v is the kinematic viscosity of the fluid under consideration) i.e. creeping flows to fully developed turbulent flows which strictly depend upon the changing wind conditions. From the engineering point of view, there are number of applications in civil, naval and mechanical engineering that employ square-cylindrical as well as circular-cylindrical structures, such as chimneys, bridges, high-rise buildings and heat exchangers. In scientific terms, the flow around multiple structures presents various important physical phenomena, such as transition, separation and vortex shedding. In this section, some of the relevant research related to vortex shedding mechanism and variation of force coefficients around circular as well as square rows of staggered arrangements is highlighted.

Before discussing staggered arrangement in detail, it is necessary to state here that no proclaimed is work reported on the hydrodynamic forces and shedding mechanism for two staggered rows of square cylinders at low Re for varying streamwise and fixing transverse spacing between the cylinders. It is cardinal to state here that the wake structures of square cylinders are remarkably different from circular cylinders for the geometry of two staggered rows. This difference is the consequence of fixed separation point of square cylinder as compared to circular cylinders where flow can separate throughout the geometry. Moreover, the hydrodynamic forces and the separation mechanism notably differ for the two geometries. Furthermore, the effect of the gap flow between the staggered cylinders, the interference effect at near wake, and far-wake emergence effect are some preponderant flow features which are needed to be addressed. However, the related numerical work remains scarce. In continuation, particular attention is paid to the numerical study of flow field and force coefficients around staggered cylinders, example of which can be found in Zdravkovich [1].

Kang [2] used immersed boundary method to study flow behavior for two side-by-side cylinders (circular) at $40 \leq Re \leq 160$ and $g^* = s/d < 5$ (where s is surface-to-surface distance in the transverse direction between cylinders). He observed that for the proposed problem the effect of g^* is much more influential than the Re. He further extended his study to three cylinders [3] and observed different flow regimes i.e. flip-flopping, single bluff-body, modulation-synchronized, deflected and in-phase synchronized for $g^* < 5$ and $Re = 100$.

Alam *et al.* [4] investigated that flow passage has constant nature of convergence and divergence for two side-by-side square cylinders as compared to circular cylinders. Guillaume and LaRue [5] experimentally and numerically examined the interacting wakes behind two and three circular cylinders aligned in side-by-side arrangement. Virahswamy *et al.* [6] used ANSYS Flotran to study the unstable gap flows behind

https://doi.org/10.1016/j.heliyon.2019.e01224

side-by-side circular cylinders. They examined asymmetrical wake flow behind the three cylinders. Wang *et al.* [7] examined the effect of equal and unequal gap spacing behind three cylinders. Zhang and Zhou [8] used laser Doppler anemometer, hot wire and flow visualization to study the effect of unequal gap spacing behind three circular cylinders for varying Re = [150−2000]. Symmetrical flow around the centerline is observed at g* = 1.5. Zhaolong *et al.* [9] examined the effect of Re = [40−160] for g* = 1.2−4. Eight different flow regimes are observed by them at different combinations of Re and g*.

Mizushima and Takemoto [10] examined the flow pattern visualization at the downstream position of a row of square cylinders. They observed that for a specific combinations of g* and Re, flopping and bi-stable flip-flop flow regimes exist. Agrawal *et al.* [11] used lattice Boltzmann method to examine different flow regimes around two side-by-side square cylinders. At Re = 73, chaotic and synchronized flow regimes are their important findings. Inoue *et al.* [12] used uniform flow to study the sound generation mechanism for flow past two side-by-side square cylinders. In another article, Inoue and Suzuki [13] extended their study to investigate the sound generation mechanism and effect of g* for flow past three side-by-side cylinders at low Re. Abbasi *et al.* [14] examined the effect of Re $\leq$ 175 for flow past an in-line square configuration for different g*. They observed steady wake pattern, stable shielding wake pattern, wiggling shielding wake pattern and vortex shedding wake pattern. Islam *et al.* [15] employed multi-relaxation-time lattice Boltzmann method to systematically compare the effect of equal and unequal gap spacing between the cylinders for flow past three side-by-side square cylinders. At Re = 150, four different flow regimes i.e. bistable, asymmetric, antiphase-modulated synchronized and modulated synchronized are observed. Rahman *et al.* [16] investigated the effect of low Re i.e. 75 to 175 and unequal gap spacing for flow past three side-by-side square cylinders. The main finding of flow regimes include flip-flopping, in-phase and anti-phase modulation synchronized, in-phase and anti-phase synchronized flow patterns. Yen and Liu [17] studied different flow structures and vortex shedding characteristics using particle image velocimetry at Re ranging from 178 to 892 and gap spacing ranging from 0 to 2.5. The authors' observed three different kinds of flow patterns: (i) single vortex-street, (ii) gap flow and (iii) couple vortex-street. They further observed that the single vortex-street flow pattern has highest Strouhal number ($St = f_s d/v$, where f_s is the vortex shedding frequency) whereas the lowest value exists for the gap-flow pattern.

The problem of wakes interaction behind multiple bluff bodies has been studied both experimentally and numerically. Mizushima and Akinaga [18] investigated the wakes and observed that the shed vortices are synchronously in-phase or anti-phase to adjacent square cylinders and this shedding depends on the gap spacing between the cylinders. Djendi [19] observed that at g* = 5, the vertical structure show breakage due to strong wake interaction amongst themselves. Kumar *et al.* [20] used

https://doi.org/10.1016/j.heliyon.2019.e01224

lattice Boltzmann method and examined synchronous, quasiperiodic, and chaotic flow patterns at $0.3 \leq g^* \leq 12$ for a fixed Reynolds number ($Re = 80$). They discussed that these flow patterns are basically the result of vortex shedding frequency (primary) and cylinder interaction frequency (secondary). Sewatkar *et al.* [21] investigated the effect of $30 \leq Re \leq 140$ and gap $1 \leq g^* \leq 4$ and proposed that the jet in the gap region strongly affect the wake interaction behind the cylinders. They also discussed that the Re has a strong effect on the wake structure mechanism especially at $g^* = 3$ and 4. Kim and Durbin [22] showed that the increasing the Re decreases the widening and narrowing of wakes. Chauve and Le Gal [23] employed visualization and biorthogonal decomposition technique to examine the wakes behind sixteen cylinders at $Re = 80$ and $g^* = 3$. They observed that the wakes which stop oscillating and appear erratically in the flow are termed as an amplitude hole. Chatterjee and Biswas [24] studied the flow behavior around staggered rows at $Re = 100$ and varying the transverse spacing between the cylinders from 1 to 5 and fixed the streamwise gap spacing equal to 1. They found the chaotic nature of flow for small transverse spacing between the cylinders. Zdravkovich and Stonebanks [25] observed that the drag forces on the upstream row of cylinders were higher than those of the downstream row of cylinders. They also found that gap flows non-uniformity disappeared beyond $T^* = T/d = 2.1$ (where T is the transverse distance between the cylinders). de Paula and Moller [26] conducted experiments to study the flow past two staggered rows of cylinders. Anagnostopoulos and Seitanis [27] investigated an aperiodic phenomena of flow past two staggered rows of circular cylinders using the finite element method at $Re = 200$. The authors' observed the formation of a large and symmetrical wake behind the downstream of cylinders at $g^* \leq 0.5$. They also observed high shedding frequencies of the upstream row of cylinders.

The scrutinizing of open literature shows that very less attention has been paid to the staggered rows of square cylinders; in particular the problem considered in this paper has not been addressed. The row of staggered square cylinders has a practical importance and is superlative case of an isolated square cylinder. It would be interesting to numerically examine how the jet flows effect the vortex shedding mechanism behind the upstream and downstream row of cylinders. In the present numerical investigation, the effect of streamwise gap spacing in the range of 0.25−2 with fixed transverse gap spacing ($T^* = 1$, 1.5 and 2) at $Re = 150$ is documented. We have also observed that the researchers separately studied the variation in the wake size [10, 23, 26, 27] and merging of jets [11, 20, 21, 24] and its effect on vortex shedding mechanism. Specifically, we argue in this paper that the jets formed between staggered rows of cylinders substantially affect the vortex shedding mechanism behind the cylinders and its corresponding force coefficients.

The paper is organized in the five different sections. In Section 2, numerical method i.e. single relaxation time lattice Boltzmann method is briefly discussed. The geometry of the prescribed problem along with boundary conditions, grid independence

https://doi.org/10.1016/j.heliyon.2019.e01224

analysis, Domain effect and code validation are given in Section 3. Results are discussed and analyzed in Section 4. Lastly, in Section 5, closure is made.

2. Methodology

The single relaxation time lattice Boltzmann method (SRT-LBM) is an explicit finite difference approximation of the Navier-Stokes equations [28]. The accuracy of this method is second-order both in time and space. Systemized parallelization, elementary execution of no-slip boundary conditions and locality of calculations make LBM attractive for flows in complex geometries [29]. This method describes the evolution of a discretized particle distribution function, $f(\mathbf{x}, t, \eta)$, which basically represents the probability of a fictitious particle in a domain $\mathbf{x}$ with a velocity η at a certain time t. A discretization of Boltzmann equation in terms of space and time, and the conversion of space velocities (η) into a finite set of velocities $\{\mathbf{e}_i\}$ gives:

$$f_i(\mathbf{x} + e_i\delta t,\ t + \delta t) - f_i(\mathbf{x},\ t) = -1\Big/\tau\Big[f_i(\mathbf{x},\ t) - f_i^{(eq)}(\mathbf{x},\ t)\Big], \tag{1}$$

where f_i is the particle distribution function having speed $\mathbf{e}_i$, $f_i^{(eq)}$ is the equilibrium distribution function, τ is the dimensionless single relaxation time parameter ($\tau = (\upsilon + 0.5)/c_s^2\delta t$) and δt is the time step. The right-hand-side of Eq. (1) is the single relaxation time Bhatnagar, Gross and Krook (BGK) collision term [30]. The equilibrium distribution function in Eq. (1) reads:

$$f_i^{(eq)} = \omega_i\rho\Big[1 + \mathbf{e}_i.\mathbf{u}\Big/c^2{}_s + (\mathbf{e}i.\mathbf{u})^2\Big/2c^4{}_s - \mathbf{u}^2\Big/2c^2{}_s\Big], \tag{2}$$

where ω_i is the weight associated with the velocity $\mathbf{e}_i$, $\mathbf{u}$ is the macroscopic velocity vector and c_s is the speed of sound. The macroscopic velocity $\mathbf{u}$ in Eq. (2) must satisfy the low Mach number requirement, i.e., $\mathbf{u}/c_s = Ma << 1$. In the present work, for two-dimensional flows, the nine-velocity model (D2Q9) is used (see Fig. 1). The D2Q9 model has the velocity vectors $\mathbf{e}_i = [e_{ix}, e_{iy}]$ where e_{ix} = (0,1,1,-1,0,1,-1,-1,1) and e_{iy} = (0,0,1,0,-1,1,1,-1,-1). The weighting coefficients are: $\omega_0 = ¼$, $\omega_1 = \ldots = \omega_4 = 1/9$, $\omega_5 = \ldots = \omega_8 = 1/36$. The non-dimensional form of speed of sound in Eq. (2) is $c_s = 0.5773$. Macroscopic quantities such as density and velocity are as follow:

$$\rho = \sum f_i, \quad i = 0, \ldots, 8, \tag{3}$$

$$\mathbf{u} = 1\Big/\rho\sum \mathbf{e}_i f_i. \quad i = 1, \ldots, 8, \tag{4}$$

The classical Navier-Stokes equation for a weakly compressible fluid in the low Mach number regime can be obtained by applying the Chapman-Enskog expansion [29]. Pressure in LBM is related to density and is calculated by using the equation of state:

https://doi.org/10.1016/j.heliyon.2019.e01224

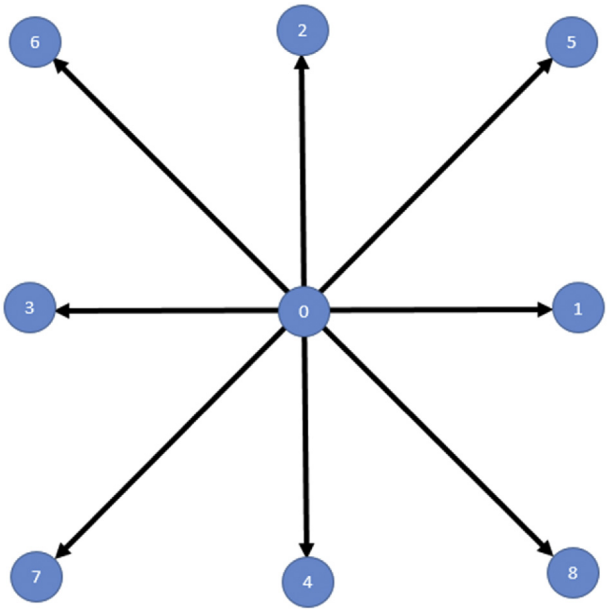

Fig. 1. D2Q9 lattice structure.

$$P = \rho c^2{}_s. \tag{5}$$

3. Design

In this section we will discuss the geometry of the proposed problem, boundary conditions, grid independence analysis, domain effect and code validation.

3.1. Problem description

The configuration for flow past two staggered rows of square cylinders of identical size d is shown in Fig. 2(a). In two-dimensional flow, seven stationary square cylinder are exposed to a uniform inflow velocity U_∞. The length of computational domain L is taken to be 44 + d. The streamwise and transverse directions are denoted as x and y, respectively. The seven cylinders are arranged from bottom to top in first row from C1 to C3 and second row from C4 to C7. H is the height of the computational domain. $L_u = 8d$ and $L_d = 34d$ are the upstream distance from the inlet to upstream row of cylinders and downstream distance from the downstream row of cylinders to exit of computational domain. T and s are the surface-to-surface distance between the cylinders in transverse and streamwise directions. An incompressible fluid having constant kinematic viscosity υ and fluid density ρ is assumed. All the important physical parameters are normalized by d, ρ and U_∞. The dimensionless time step is defined as Time $= U_\infty t/d$. The flow-induced force acting on the surfaces of cylinders are decomposed into F_x and F_y, and the drag and lift coefficients are defined as $C_d = 2F_x/\rho U_\infty^2 d$ and $C_l = 2F_y/\rho U_\infty^2 d$,

https://doi.org/10.1016/j.heliyon.2019.e01224

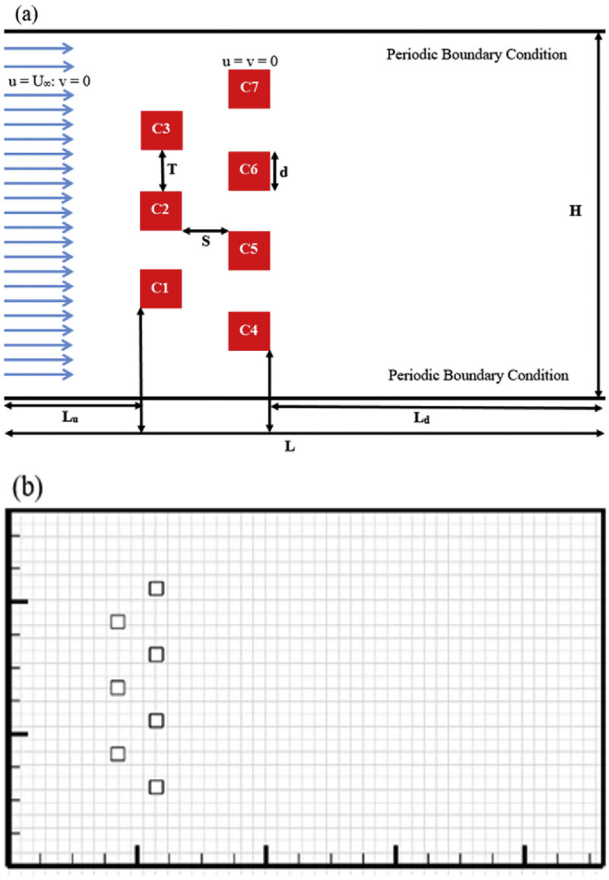

Fig. 2. (a, b). The computational domain and Grid distribution.

respectively. The code for this problem was written and edited using Compaq Visual Fortran version 6.5.0. The chosen grid distribution for different g* and T* are given in Table 1. The grid distributions for one specific case at T* = 1.5 and g* = 2 is presented in Fig. 2(b).

Table 1. Grid distribution for different T* and g* at Re = 150.

T*	g*	L × H	T*	g*	L × H	T*	g*	L × H
1.0	0.25	886 × 481	1.5	0.25	886 × 541	2.0	0.25	886 × 601
	0.5	891 × 481		0.5	891 × 541		0.5	891 × 601
	0.75	896 × 481		0.75	896 × 541		0.75	896 × 601
	1.0	1001 × 481		1.0	1001 × 541		1.0	1001 × 601
	1.25	1006 × 481		1.25	1006 × 541		1.25	1006 × 601
	1.5	1011 × 481		1.5	1011 × 541		1.5	1011 × 601
	1.75	1016 × 481		1.75	1016 × 541		1.75	1016 × 601
	2.0	1021 × 481		2.0	1021 × 541		2.0	1021 × 601

https://doi.org/10.1016/j.heliyon.2019.e01224

3.2. Boundary conditions

An inlet of the channel is exposed to a uniform inflow velocity ($\mathbf{u} = U_\infty$, $\mathbf{v} = 0$). At the outlet position, the convective boundary condition was used for all velocity components [31]. No-slip boundary condition ($\mathbf{u} = \mathbf{v} = 0$) using the bounce-back role was enforced at the body surfaces [31]. At the upper and lower boundaries of computational domain periodic boundary conditions were used in the transverse direction [32]. To obtain an accurate torque and hydrodynamic forces on the solid body immersed in a fluid flow, we have employed the momentum exchange method [33, 34].

3.3. Grid independence analysis

In order to investigate the grid independence analysis, computations are performed for flow past a single square cylinder. The mean drag coefficient (Cdmean) and Strouhal number are computed and given in Table 2 together with percentage variation. The maximum percentage variation of the mean drag coefficient between d = 10 and d = 20 are found to be within 3.6%, whereas for the d = 20 and d = 40 are within 0.24%. Similarly, the maximum percentage variation of the Strouhal number between d = 10 and d = 20 are found to be within 4.5%, whereas for the d = 20 and d = 40 are within 0.2%. Hence d = 20 grid is chosen for all computations.

3.4. Domain effect

The domain effect for flow past a single square cylinder are given in Table 3 with percentage variation of mean drag coefficient, Strouhal number and root-mean-square value of lift coefficient (Clrms). It is found that case II is the best choice for current numerical study as compared to other mentioned cases in Table 3.

3.5. Code validation

To validate the accuracy of present numerical method, the simulations for flow over single square cylinder at Re = 150 is executed. The comparison of the Cdmean and

Table 2. Grid independence analysis at Re = 150 for flow past a single square cylinder.

d	Cdmean	St
10	1.4521	0.1498
	(3.6%)	(4.5%)
20	1.4020	0.1565
	(0.24%)	(0.2%)
40	1.3986	0.1562

https://doi.org/10.1016/j.heliyon.2019.e01224

Table 3. Domain effect g* at Re = 150 for flow past a single square cylinder.

Cases	Grid Sizes	Cdmean	St	Clrms
I	L_u = 5d; L_d = 34d; H = 12d	1.4321	0.1486	0.2348
II	L_u = 8d; L_d = 34d; H = 12d	1.4020	0.1565	0.2528
III	L_u = 12d; L_d = 34d; H = 12d	1.3986	0.1563	0.2521
IV	L_u = 8d; L_d = 22d; H = 12d	1.4216	0.1520	0.2465
V	L_u = 8d; L_d = 45d; H = 12d	1.4012	0.1565	0.2456
VI	L_u = 8d; L_d = 34d; H = 8d	1.4186	0.1545	0.2456
VII	L_u = 8d; L_d = 34d; H = 15d	1.3998	0.1565	0.2549

St for flow past a single square cylinder with others published data are presented in Table 4. It is found that the present numerical results are in good agreement with other published data [20, 24, 35, 36], which proves that our numerical method is accurate to study the proposed problem.

In order to further validate the numerical code, simulations are carried out for flow past single square cylinder at Re = 20 and x-velocity profile is compared with the findings of Wang et al. [37]. Results are found in good agreement (see Fig. 3) with slight discrepancies which appear due different choice of physical parameters like geometry of cylinder, computational domain, boundary conditions etc. Since we are dealing with square cylinder which has fixed separation points while Wang et al. [37] has dealt with circular cylinder where any point on cylinder can act as a separation point. These tests of grid convergence, effect of computational domain and code validation developed our confidence in the use of present code for studying the flow past two staggered rows of square cylinders.

We also numerically examine the effect of number of cylinders required to simulate a flow past a row of cylinders. Computations are done for g* = 4 and Re = 80 to compare our results with Kumar *et al.* [20]. Table 5 shows that drag coefficient is almost invariant when 7 or more cylinders are present in the flow field. The seven square cylinders of same size are chosen for present study. Overall a good agreement is observed between the present results and Kumar *et al* [20].

Table 4. Comparison of aerodynamic characteristics data for a single square cylinder at Re = 150.

Present	Cdmean	St
	1.4020	0.1565
Kumar *et al.*[20]	1.5260	0.1562
Chatterjee and Gupta[24]	1.4400	0.1606
Gera *et al.*[35]	1.4110	0.1410
Sohankar *et al.*[36]	1.4100	0.1610

https://doi.org/10.1016/j.heliyon.2019.e01224

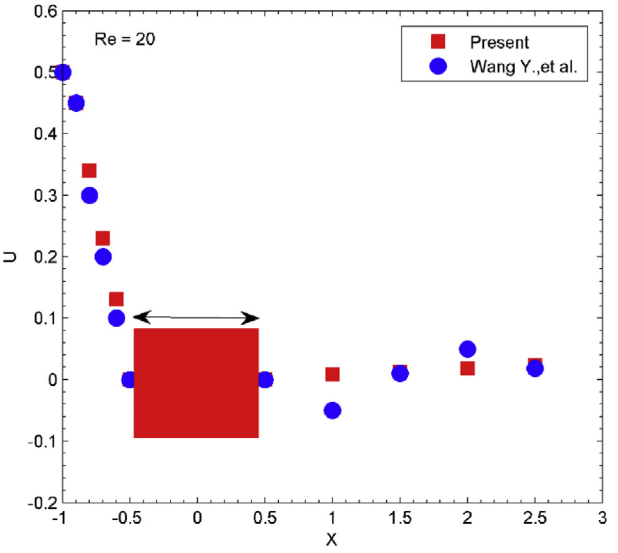

Fig. 3. Comparison of x-velocity profile.

Table 5. Comparison of mean drag coefficient from row of four, seven and nine identical square cylinders for flow past side-by-side square cylinders at g* = 4 and Re = 80.

Number of cylinders		Cdmean
4	Present	1.7231
	Kumar *et al.*[20]	1.7050
7	Present	2.0140
	Kumar *et al.*[20]	1.9150
10	Present	2.0210
	Kumar *et al.*[20]	1.9160

4. Results & discussion

The spacings in the transverse direction, T*, were held fixed equal to 1, 1.5 and 2. The computations are comprised of eight spacings in the streamwise direction, g*, namely 0.25, 0.5, 0.75, 1, 1.25, 1.5, 1.75 and 2. The first row containing three cylinders was located upstream of the four-cylinder row in the downstream direction. When the upstream and downstream rows of cylinders aligned for g* = 0, they form a single row of seven cylinders.

The Strouhal number was calculated by performing a Fast Fourier Transform (FFT) of the time history of lift coefficients of all cylinders. The highest peak in the spectrum gives the Strouhal value which is called the primary vortex shedding frequency. In case of multiple peaks the other peaks are called the secondary cylinder interaction frequency (SCIF). The idea of SCIF was studied by Kumar *et al.* [20]. They

https://doi.org/10.1016/j.heliyon.2019.e01224

observed that this frequency corresponds to the time interval in which the narrow wake behind one cylinder becomes wide before becoming narrow again.

In this study, we observed that calculated values of mean drag coefficient (Cdmean) Strouhal number (St), root-mean-square values of drag (Cdrms) and lift coefficients (Clrms) show similar behavior for specific pair of cylinder across the center line of computational domain. This similarity predominantly originates between two pairs of cylinders i.e. (C4, C7) and (C5, C6) and found to be greatly influenced by streamwise and transverse gap spacings. Based on this observation the time-trace study of drag and lift coefficients and force statistics data is given for all seven cylinders whereas power spectra analysis of lift coefficients for cylinders C1, C2, C6 and C7 is provided. It is important to state here that the dashed and solid lines in the vorticity contours visualization plots represented the negative and positive vortices generating from the upper and lower corners of the cylinders, respectively. In case of signal of time-trace analysis of drag coefficients, one can see only the dashed-dotted line for cylinders (C4, C7) and (C5, C6) because both of them have same drag amplitude whereas signal of time-trace analysis of lift coefficients also have dashed-dotted lines that appear as a a mirror image for (C1, C3), (C4, C7) and (C5, C6).

A vorticity snapshot of the flow field illustrating different vortex shedding patterns for two staggered rows of cylinders is reported in Fig. 4(a−d) for different g* values at T* = 1. The flip-flopping vortex shedding mechanism is clearly seen for smaller streamwise gap spacings (g* = 0.25 and 0.75) (see Fig. 4(a, b)). The shed vortices are not clear in the vicinity downstream row of cylinders. It is observed that some of the shed vortices behind the downstream row of cylinders are narrower or wider than the normal shed vortices. This is due to the strong flow interference between successive cylinders at small streamwise gap spacings. Furthermore, the jets behind row of cylinders are merging. The wake structure mechanism behind downstream row of

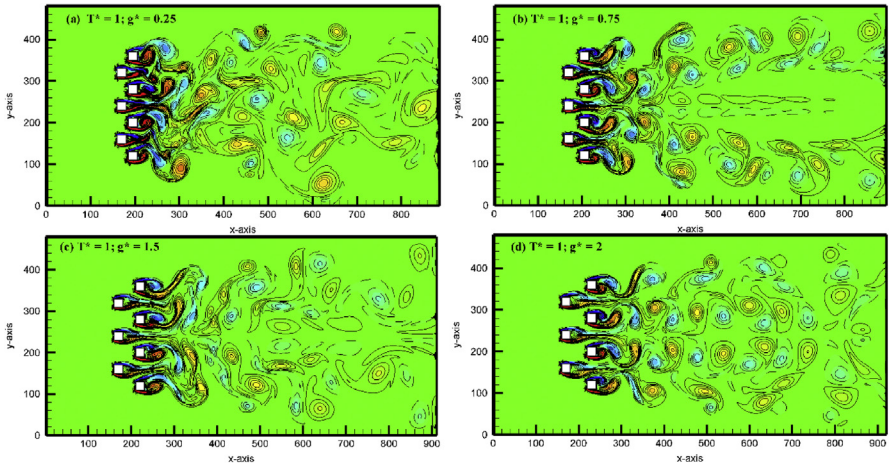

Fig. 4. Vorticity snapshots for (a) g* = 0.25, (b) g* = 0.75, (c) g* = 1.5 and (d) g* = 2 at T* = 1.

https://doi.org/10.1016/j.heliyon.2019.e01224

cylinders is quite identical with that of Kumar *et al.* [20] obtained numerically for flow past nine side-by-side square cylinders in a single row at g* = 1. Similar characteristics are observed for T* = 1 and g* = 0.5 (not shown). At small downstream distance (x/d ≈ 2) behind the downstream row of cylinders the vortices coalesce together and as a result some of the wakes appear narrower and wider as compared to wake behind isolated cylinder. For example in Fig. 4(c), the wake behind cylinder C1 is wider and that behind cylinder C2 is narrower. This effect almost becomes vanished at sufficiently large streamwise gap spacings (Fig. 4(d)). In all cases with g* ≤ 0.75, the vortex interactions that took place just behind the downstream row of cylinders were notably different from those in the near wake of upstream row of cylinders, as one can clearly see in Fig. 4(b, d). The present numerical results are in good agreement with the experimental observation of Cheng and Moretti [38]. They also observed that some of the wakes may be very wide behind the cylinders. Similar flow features are obtained for g* = 1 and 1.25 and also for g * = 1.5 (not shown).

The above observations regarding to different vortex shedding mechanism can also be verified in Fig. 5 by looking into the time-trace study of the drag (Cd) and lift coefficients (Cl) of cylinders (C1−C7). Fig. 5(c, d, g, h, k, l, o, p) for chosen g* value shows that lift coefficients are sinusoidal in nature. The signals of lift coefficients for pair of cylinders (C1, C3), (C4, C7) and (C5, C6) for both upstream and downstream row of cylinders appears to be a mirror image (Fig. 5(c, g, k, o)). The amplitude of both drag and lift signals show a fluctuating behavior at small streamwise gap spacings and become almost constant at large streamwise gap spacing. This shows that both drag and lift coefficients are decoupled at smaller streamwise gap spacings (g* = 0.25 and 0.75) as compared to larger streamwise gap spacings (g* = 1.5 and 2). Fig. 5(a, b, e, f, i, j, m, n) for chosen g* value shows that drag coefficients. It is observed that the signal of drag coefficients of the downstream row of the cylinders i.e. (C4, C7) and (C5, C6) are the same at g* = 0.75, 1.5, 2 see Fig. 5(f, j, n).

Fig. 6(a−m) shows the spectrum analysis of the lift coefficients for various streamwise gap spacings i.e. g* = 0.25, 0.75, 1.5 and 2 at fixed T* = 1. In case of large streamwise gap spacing weak interaction vortex shedding mechanisms are observed due to negligible cylinders interactions. As a result one can clearly see the distinct peak in the power spectrum (Fig. 6(e−m)). In case of g* = 2, single peak is observed at St = 0.1679, 0.1667, and 0.1667 for cylinders C1, C6 and C7, respectively (Fig. 6(m−p)). Graphical representation of C2 for g* = 0.75, 1.5, 2 is not given because it appears to be a straight line. This phenomenon occurs because signal of lift coefficient for such cases is also a straight line see Fig. 5(g, k, o). Additionally, peaks at the left of highest peak 0.1659, 0.1659 and 0.1659 for cylinders C1, C6, and C7 are actually the superharmonics. Similarly some superharmonics exist on the right side also. The power spectrum analysis clearly reveals that the vortex shedding process is totally dominated by the primary vortex shedding frequency at g* ≥ 0.75 and no secondary cylinder interaction frequency effects occur at larger streamwise

https://doi.org/10.1016/j.heliyon.2019.e01224

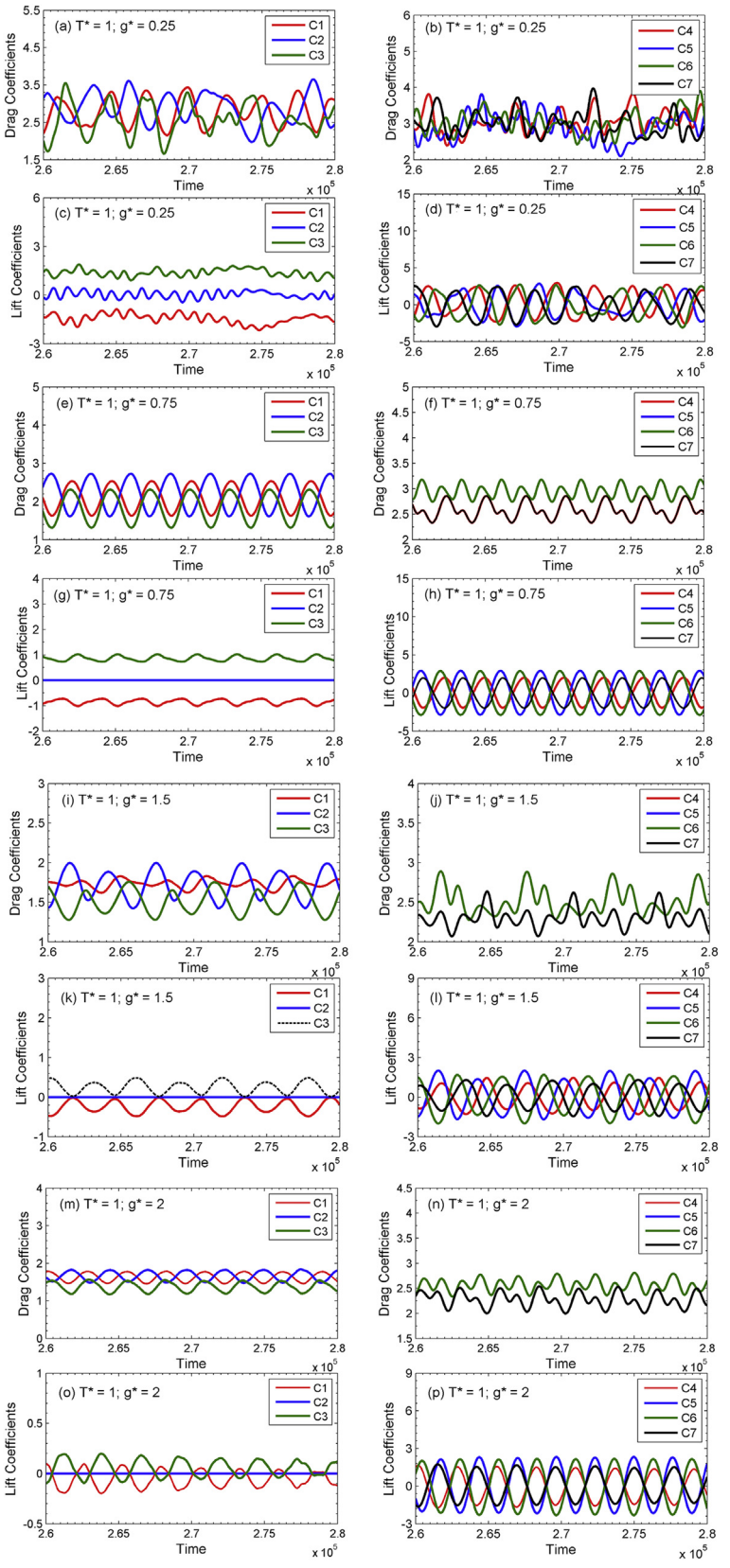

Fig. 5. Time-trace study of Cd and Cl for T* = 1: (a, b, e, f, i, j, m, n) C1−C7 cylinders drag versus time for different g*, and (c, d, g, h, k, l, o, p) C1−C7 cylinders lift versus time for different g*.

https://doi.org/10.1016/j.heliyon.2019.e01224

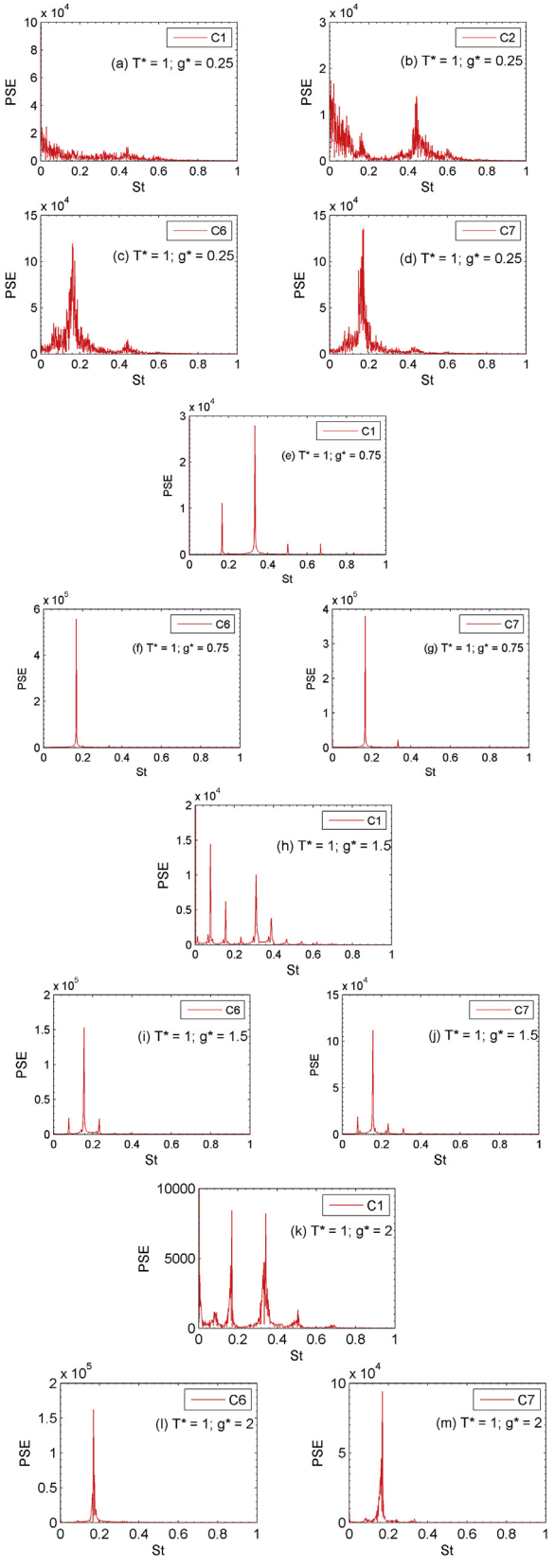

Fig. 6. Power spectra analysis of C1, C2, C6 and C7 for T* = 1: (a–d) g* = 0.25, (e–g) g* = 0.75, (h–j) g* = 1.5 and (k–m) g* = 2.

https://doi.org/10.1016/j.heliyon.2019.e01224

gap spacing. At g* = 0.25, the combination of the PVSF and SCIF leads to multi peaks as presented in Fig. 6(a–d). It is clear from the time signal of lift coefficient for g * = 0.25 (see Fig. 5(b)).

Now the vorticity snapshots at T* = 1.5 for various streamwise gap spacings are shown in Fig. 7(a–d). The vortices shedding behind the downstream rows of cylinders do not remain distinct at g* = 0.25 and 0.75 (Fig. 7(a, b)), because of the strong interactions and due to relatively small streamwise gap spacing between the upstream and downstream row of cylinders. As a result, the shed vortices reveal some in-phase and anti-phase behavior. The similar vortex shedding behavior is observed for g* = 0.5 and 1 (not shown). For relatively large gap spacing g* = 1.25 and 2 nearly modulated synchronized vortex shedding mechanism is observed for downstream row of cylinders and almost nearly unsteady behavior for upstream row of cylinders (Fig. 7(c, d)). The shed vortices behind the downstream row of cylinders remain distinct throughout the computational domain. Similar vortex shedding characteristics are observed for g* = 1.5 and 1.75 (not shown). Kang[3] had similar observations for flow past three side-by-side circular cylinders at Re = 100. It is also observed that the gap vortices and those separated from the inner and outer sides of the cylinders strongly interact behind the downstream row of cylinders and play a role in destabilizing and distortion of shed vortices (Fig. 7(a)). The almost symmetrically-biased flow characteristics are observed due to gap flow biased/diverged outward or inward between the cylinders (Fig. 7(c)). A wide wake is observed behind the middle cylinder (C2) and a narrow wake is observed behind lower (C5) and upper (C6) cylinders. The vortices generating from by the upstream row of cylinders switches the direction (up and down), and this affect basically controlled by the wakes generated behind the downstream row of cylinders.

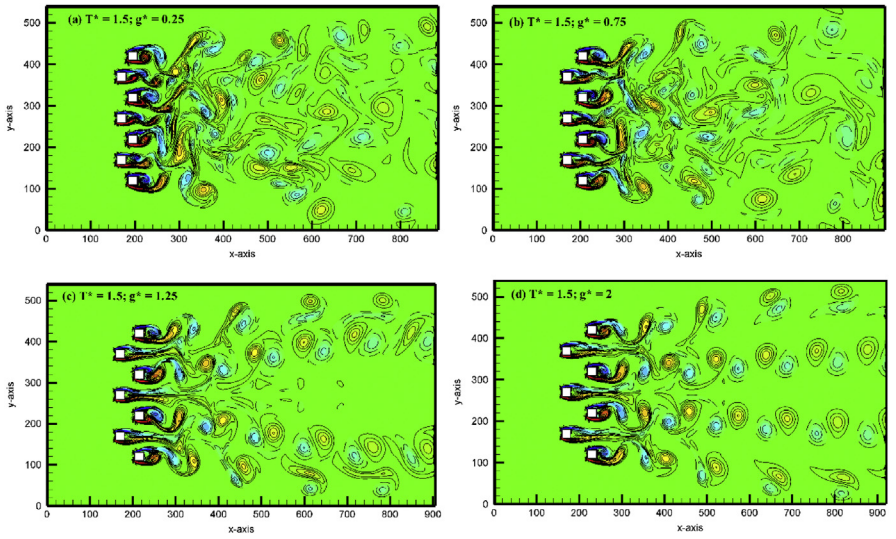

Fig. 7. Vorticity snapshots at (a) g* = 0.25, (b) g* = 0.75, (c) g* = 1.25 and (d) g* = 2 at T* = 1.5.

https://doi.org/10.1016/j.heliyon.2019.e01224

One can clearly see that the shed vortices generated from cylinder C1 is displaced slightly upward due to the wide wake of cylinder C5. Furthermore, the wake is tilted downwards behind cylinder C2, guided by the vorticity generated from cylinder C5. The same phenomena has been observed by Alam *et al.* [4] for two side-by-side square cylinders. In addition, the vortex shedding mechanism in near wakes for $g^* \geq 1.25$ is very similar, qualitatively to in the near wake of the flow past a single square cylinder for all cylinders except cylinder C2.

At $g^* = 0.25$, 0.75, 1.25 and 2, the time-trace analysis of drag and lift coefficients for cylinders (C1−C7) are shown in Fig. 8(a−p). There is significant variation in the signal for upstream row (C1, C2 and C3) and downstream row of cylinders (C4, C5, C6 and C7) at small $g^* = 0.25$, 0.75. Also the signals of drag coefficient of cylinder (C4, C7) and (C5, C6) hinder the overlapping due to the strong merging and distortion of shed vortices Fig. 8(a, b, e, f, i, j, m, n). At $g^* = 1.25$ and 2 (Fig. 8(i, j, m, n)), a wide wake is observed behind cylinder C1 which provides justification for the low drag on these cylinders (Cdmean = 1.7986 and 1.628 for $g^* = 1.25$ and 2, respectively), whereas the medium size wake is observed behind cylinders C4 and C2. The wake behind cylinder C2 is similar to the wake observed behind cylinder C1 although somewhat narrower, which results in a slightly higher drag (Cdmean = 1.6619 and 1.8443 for $g^* = 1.25$ and 2, respectively). The drag coefficient signals do not resemble the. It shows a modulated sine for drag coefficients. We also observed that the lift forces show sinusoidal variation Fig. 8(c, d, g, h, k, l, o, p).

The power spectra of Cl at $T^* = 1.5$ for different g^* values are presented in Fig. 9(a−n). The multiple peaks in the spectrum are the linear combination and harmonic occurring due to the presence of jet flow between the cylinders (see Fig. 9(a−h)). The lift coefficient signals for $g^* = 0.25$ and 0.75 (Fig. 8(b, d)) clearly indicate the presence of secondary cylinder interaction frequency. This is further confirmed from the power spectrum analysis shown in Fig. 9(a−h). On the other hand, the signal of lift coefficient at $g^* = 1.25$ and 2 (Fig. 8(f, h)) shows the presence of only primary vortex shedding frequency (Fig. 9(i−n)) except for cylinder C2 at $g^* = 1.25$, 2.

At $T^* = 2$, Fig. 10(a−d) show the vorticity snapshots for different streamwise gap spacings. For $g^* = 0.25$, the shed vortices are seen up to $x/d \approx 6$ and coalesce with each other is observed at further downstream of the computational domain (see Fig. 10(a)). A similar observation is applied at $g^* = 0.5$ and 0.75 (not shown). The fully generated wakes from the upstream row of cylinders alternately attaches and detaches behind the downstream row of cylinders. Due to negligible jet flow effect and shear layers generated from the upstream row of cylinders, the vortex shedding pattern behind the downstream row of cylinders are showing in-phase or anti-phase behavior (Fig. 10(b−d)). For $g^* = 2$, almost the similar behavior is observed for cylinder C2. For $g^* = 1.25$ and 2, the interaction between shed vortices in the

https://doi.org/10.1016/j.heliyon.2019.e01224

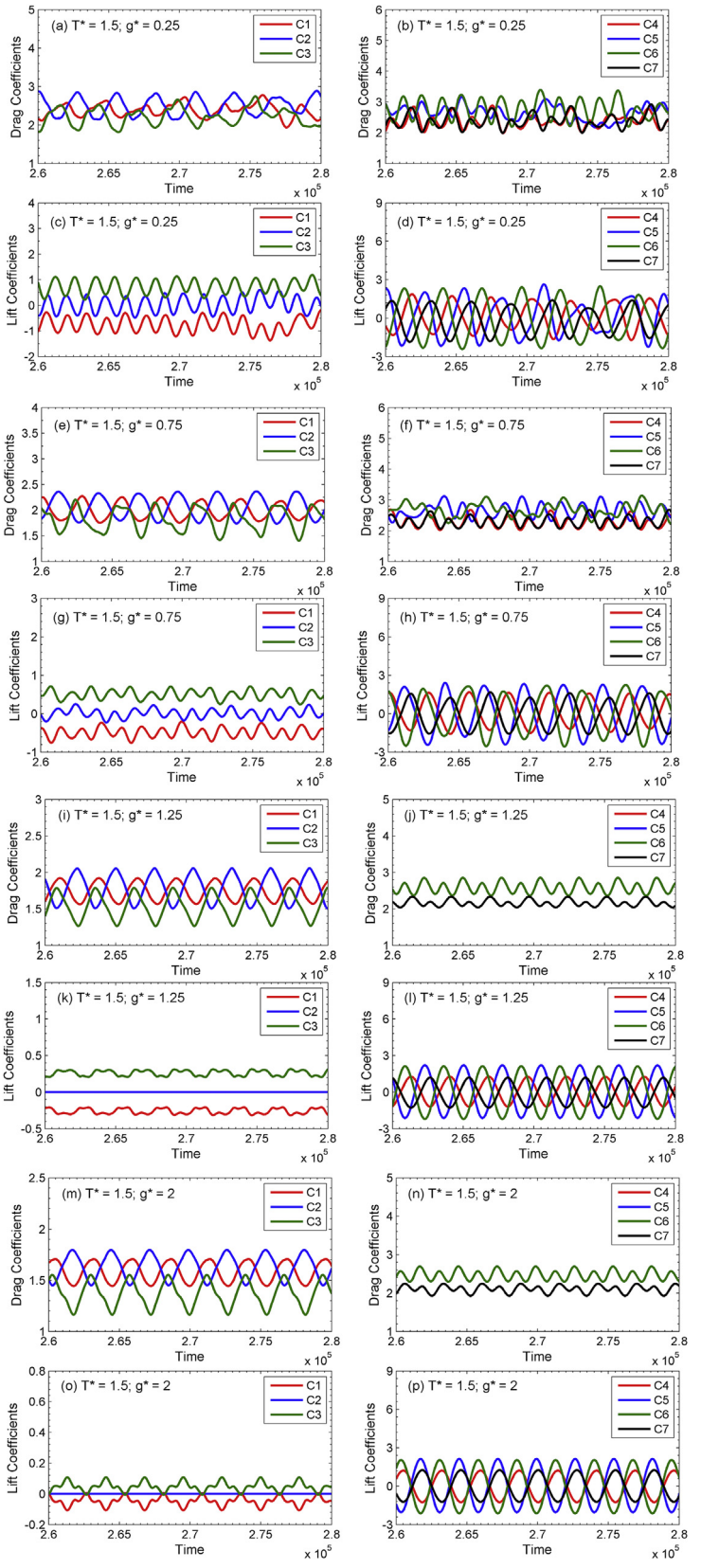

Fig. 8. Time-trace study of Cd and Cl for T* = 1.5: (a, b, e, f, i, j, m, n) C1−C7 cylinders drag versus time for different g*, and (c, d, g, h, k, l, o, p) C1−C7 cylinders lift versus time for different g*.

https://doi.org/10.1016/j.heliyon.2019.e01224

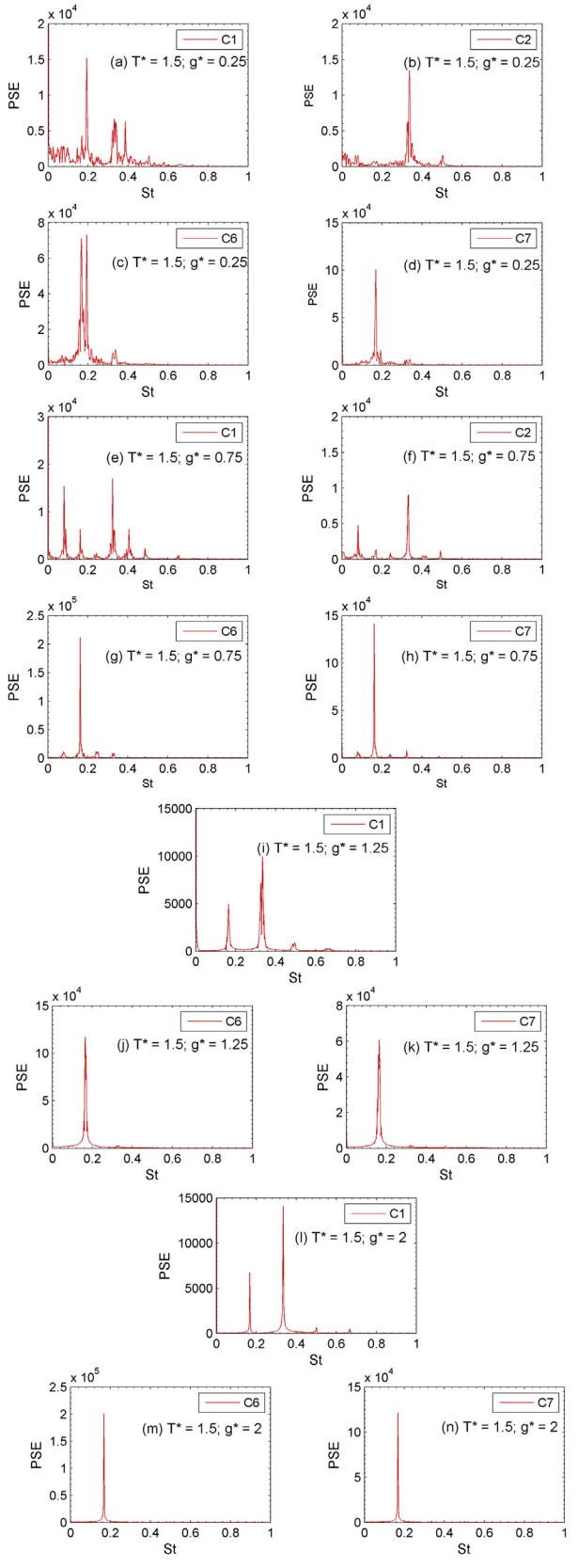

Fig. 9. Power spectra analysis of C1, C2, C6 and C7 for T* = 1.5 for (a–d) g* = 0.25, (e–h) g* = 0.75, (i–k) g* = 1.5 and (l–n) g* = 2.

https://doi.org/10.1016/j.heliyon.2019.e01224

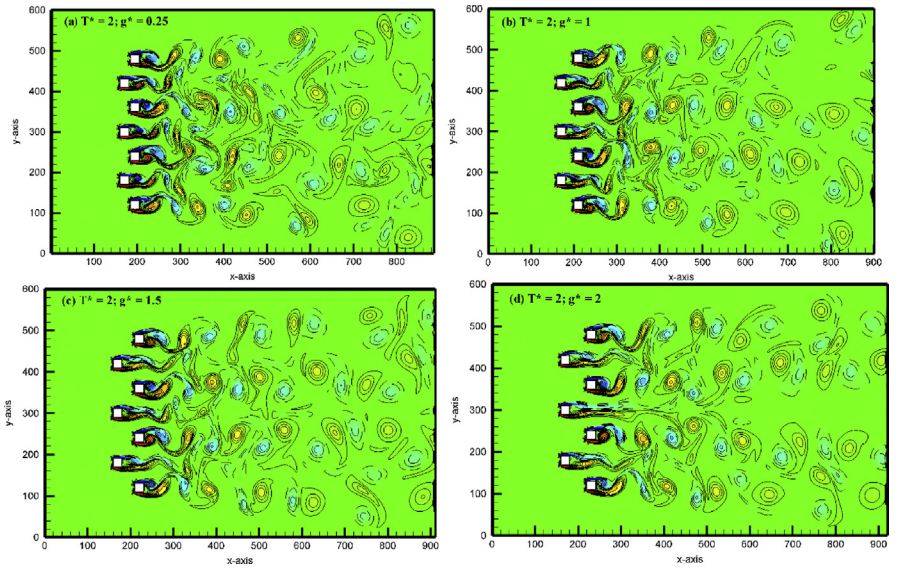

Fig. 10. Vorticity snapshots for T* = 2 at four different streamwise gap spacings: (a) g* = 0.25, (b) g* = 1, (c) g* = 1.5 and (d) g* = 2.

near wakes of the upstream and downstream row of cylinders became weaker and the shed vortices originating from the downstream row of cylinders neither significantly pulled towards the wake of upstream row of cylinders nor deformed. At g* = 1 (see Fig. 10(b)), the wake behind cylinder C6 is wider than that behind other cylinders and the shedding of vortices are almost in-phase for cylinders C2 and C6. The in-phase vortex shedding behind cylinders C2 and C6 is compatible to the in-phase behavior of the lift coefficient signal of these two cylinders. If we consider only cylinders C1, C4 and C5, in case of g* = 1.5 and 2 (Fig. 10(c, d)), the cylinder wakes becomes modulated synchronized. It is observed that the modulation occurs and is large when compared to vortex shedding. The generated shed vortices behind cylinders C4 and C5 are not affected and thus show an anti-phase characteristics. Mizushima and Akinaga[18] had similar observations for flow past row of square cylinders in presence of uniform flow.

The observations about modulated synchronized in-phase/antiphase are studied for T* = 2 by varying the values of g* and are supported by the time histories of drag and lift coefficients of cylinders (C1−C7) in Fig. 11(a−p). The lift coefficients amplitude is constant with a zero mean for all cylinders (Fig. 11(c, d, g, h, k, l, o, p)). Approximatelly in-phase charcateristics of lift coefficients are observed for cylinders C4 and C6. Evidence of vortex shedding behind the downstream row of cylinders with phase difference is also observed from the time-trace study of drag coefficient signals (Fig. 11(a, b, e, f, i, k, m, n)).

The different flow characteristics have been demorcated based on the spectra analysis of Cl, at various T* and g* shown in Fig. 12(a−p). The small peaks in the

https://doi.org/10.1016/j.heliyon.2019.e01224

spectra analysis of lift coefficients for g* = 2 (see Fig. 12(m−p)) are belived to correspond to SCIF. A Strouhal number corresponds to the PVSF, whereas the multi are its harmonics. These observations are in good agreement with the numerical work of Kumar *et al.* [20] for flow across nine side-by-side square cylinders at g* = 2 and Re = 80. The dominant PVSF in Fig. 12(a−p) clearly indicates the independent movement of shed vortices behind the cylinders. Chatterjee and Biswas[24] also observed the presence of PVSF at large gap spacing for flow past row of side-by-side square cylinders at g* = 0.

The dependence of some important physical parameters such as Cdmean, St, Cdrms and Clrms on the streamwise gap spacing for fixed value of T* have been evaluated and shown in Figs. 13(a−f), 14(a−f), 15(a−f), 16(a−f), respectively. It is observed that Cdmean shows a decreasing behavior while increasing the streamwise gap spacing. Also mean drag coefficient of C1, C2, C3 approaches to single cylinder case at large streamwise gap spacing. This is due to the flow separation appearing at the sharp corners. It is interesting to note that the Cdmean value of cylinders decreases to their minimum value by increasing the value of g*. On the other hand, at T * = 2 and for all chosen g*, the values of Cdmean for cylinders C4, C5, C6, C7 are very much lower as compared to that of a single square cylinder, which means that the interference from the upstream row of cylinders to downstream row of cylinders becomes relatively weak.

The Strouhal number, however, shows almost insensitive behavior for both upstream and downstream rows of cylinders. Some irregularities are observed at T* = 1 and g* = 0.25, 0.5 and T* = 1.5 and g* = 0.25, 0.5, 0.75 for cylinder C2 where strouhal number show asymmetrical behavior and get vanished for remaining streamwise gap spacing. This phenomenon occurs due to the steady behavior of flow around C2 for these particular gap spacings. It is important to notice that maximum St occurs for upstream rows of cylinders at T* = 2 for all selected streamwise gap spacings. The cylinder C2 attains its minimum value for g* = 0.25 at T* = 1 (Fig. 14(a)) due to merging of shed vortices. As compared to mean drag coefficient, the Strouhal values almost approaches to single cylinder value except for cylinders C2 at T* = 1 and g* = 0.25, 0.5 and T* = 1.5 and g* = 0.25, 0.5, 0.75 and T* = 2 for all g* (Fig. 14(a, b, c)).

The Cdrms data of all seven cylinders show a mixed trend i.e. an increasing and decreasing behavior while increasing the transverse and streamwise gap spacings (Fig. 15(a−f)). In transverse case of T* = 1.5, combination of T* = 1.5 and g* = 1 have maximum values of Cdrms for all seven cylinders and at T* = 1.5 and g* = 2 Cdrms has a minimum values. The cylinder C5 and C6 have maximum values of Cdrms at T* = 2 for all chosen combination of transverse and streamwise

https://doi.org/10.1016/j.heliyon.2019.e01224

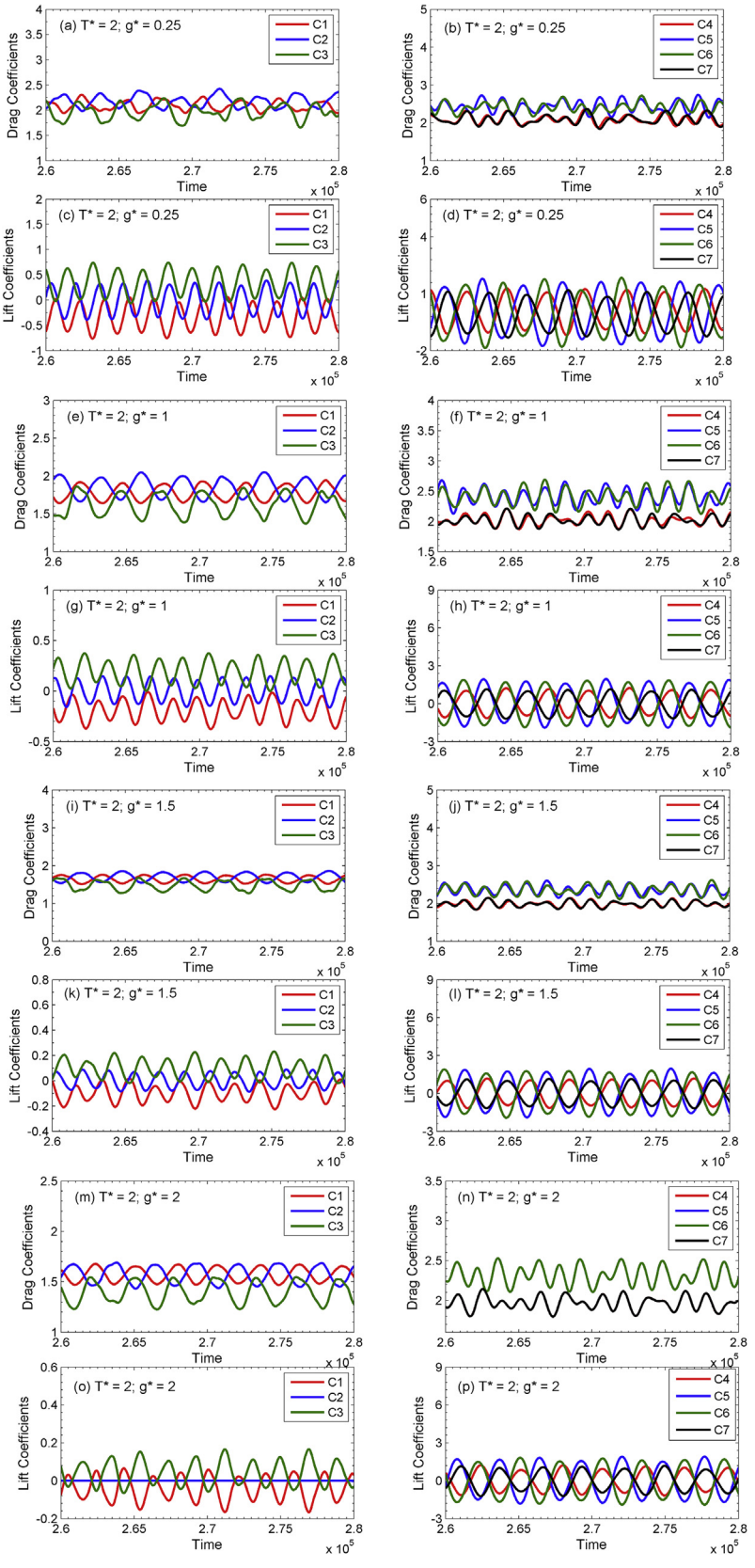

Fig. 11. Time-trace study of Cd and Cl for T* = 2: (a, b, e, f, i, j, m, n) C1−C7 cylinders drag versus time for different g*, and (c, d, g, h, k, l, o, p) C1−C7 cylinders lift versus time for different g*.

https://doi.org/10.1016/j.heliyon.2019.e01224

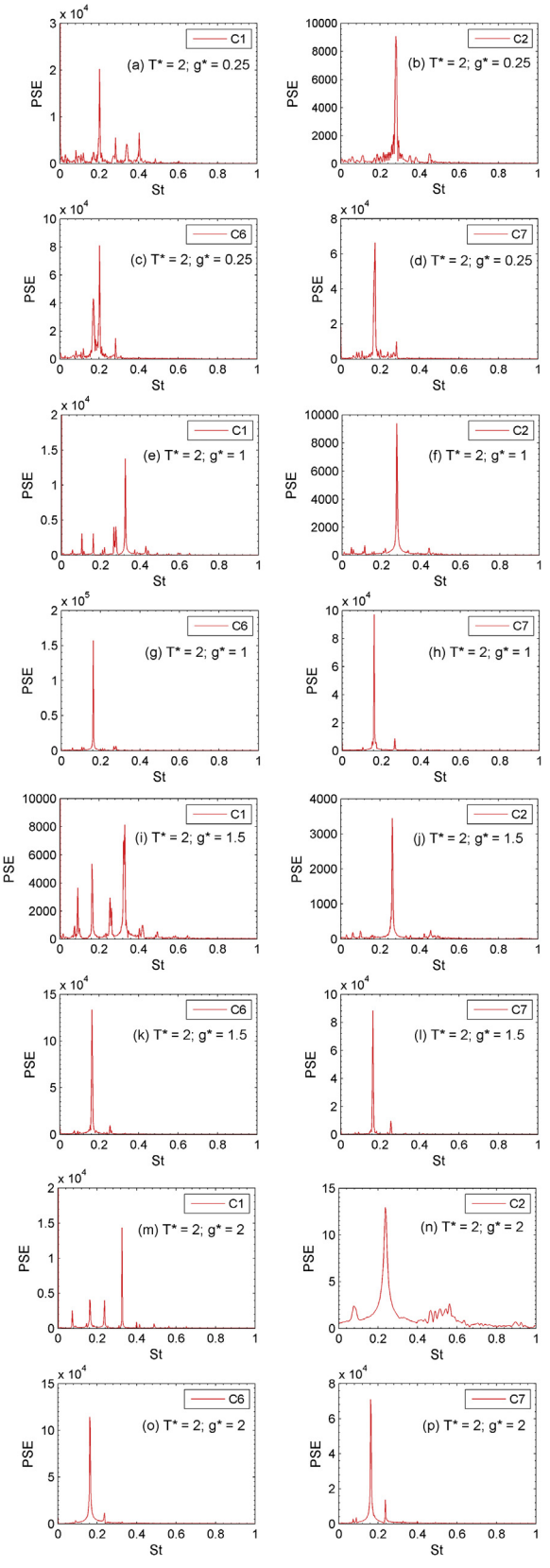

Fig. 12. Power spectra analysis of C1, C2, C6 and C7 for T* = 2 (a–d) g* = 0.25, (e–h) g* = 1, (i–l) g* = 1.5 and (m–p) g* = 2.

https://doi.org/10.1016/j.heliyon.2019.e01224

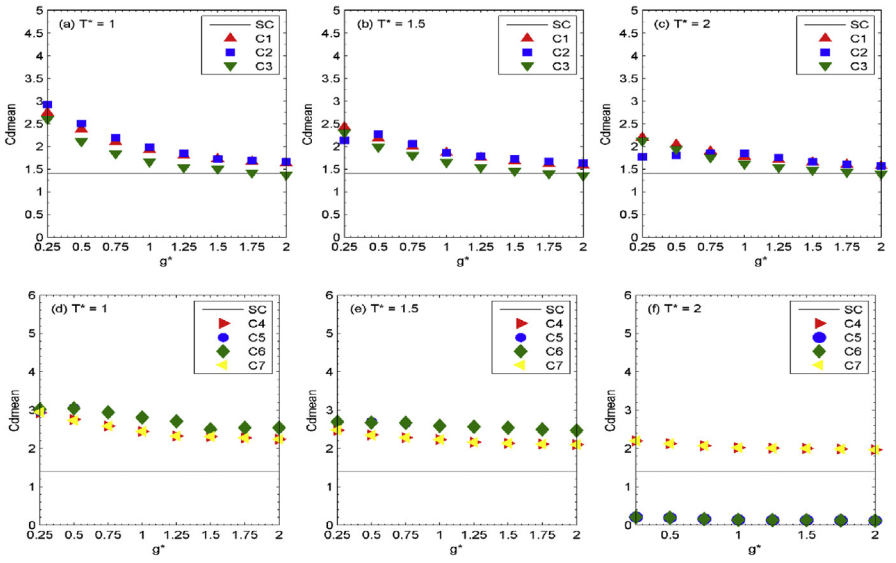

Fig. 13. Comparison of mean drag coefficient as a function of g* for different T* values (a, d) T* = 1, (b, e) T* = 1.5 and (c, f) T* = 2.

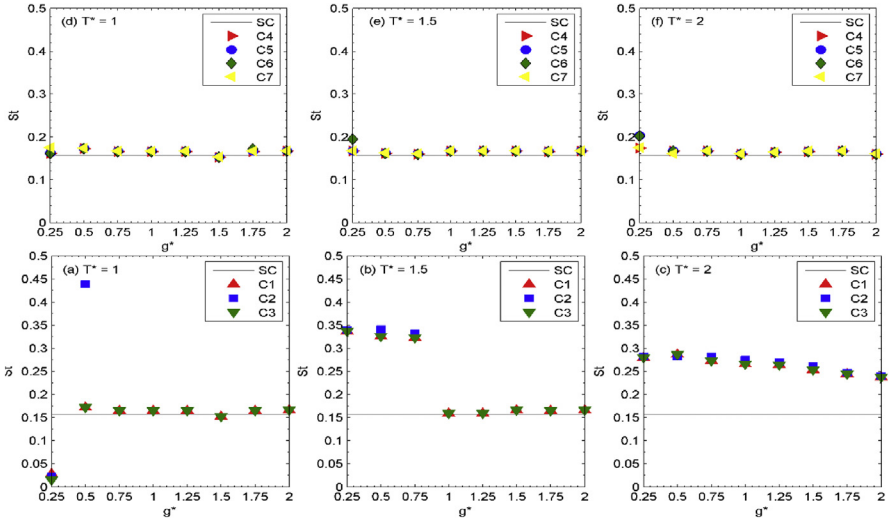

Fig. 14. Variation of Strouhal number by varying the values of g* for different fixed T* values (a, d) T* = 1, (b, e) T* = 1.5 and (c, f) T* = 2.

gap. It is also observed that pairs of cylinder from downstream row of cylinders i.e. (C4, C7) and (C5, C6) show same behavior of Cdrms for all T* and g*. It is also observed that Cdrms values of all seven cylinders approaches the single cylinder case at large streamwise gap spacings except for C5 and C6 at T* = 2.

In case of T* = 1, 1.5 and 2, the Clrms value of upstream row of cylinder are below than the value of single square cylinder (Fig. 16(a−c)). Similarly, at T* = 2 and for cylinder C5 and C6 of downstream row of cylinder have also values below than the

https://doi.org/10.1016/j.heliyon.2019.e01224

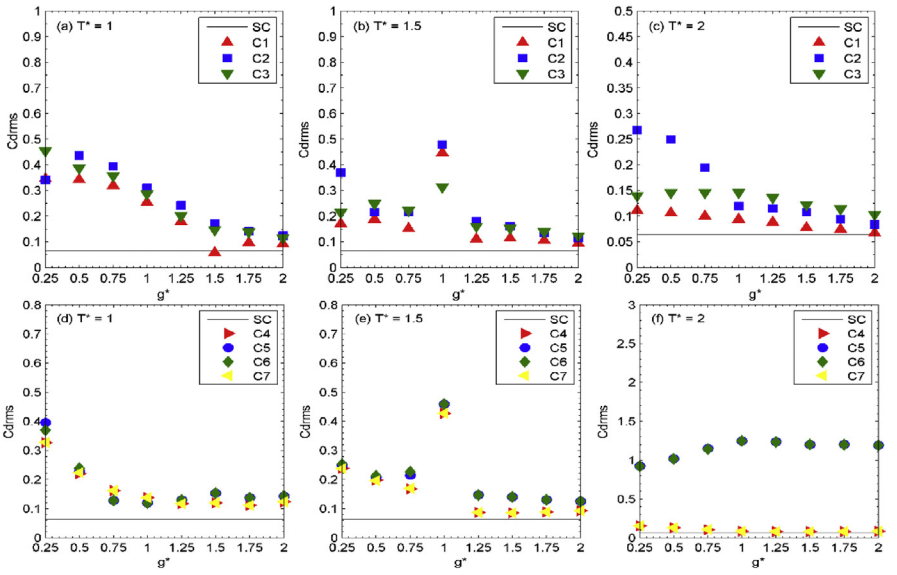

Fig. 15. Comparison of root-mean-square value of drag coefficient as a function of g* for different T* values (a, d) T* = 1, (b, e) T* = 1.5 and (c, f) T* = 2.

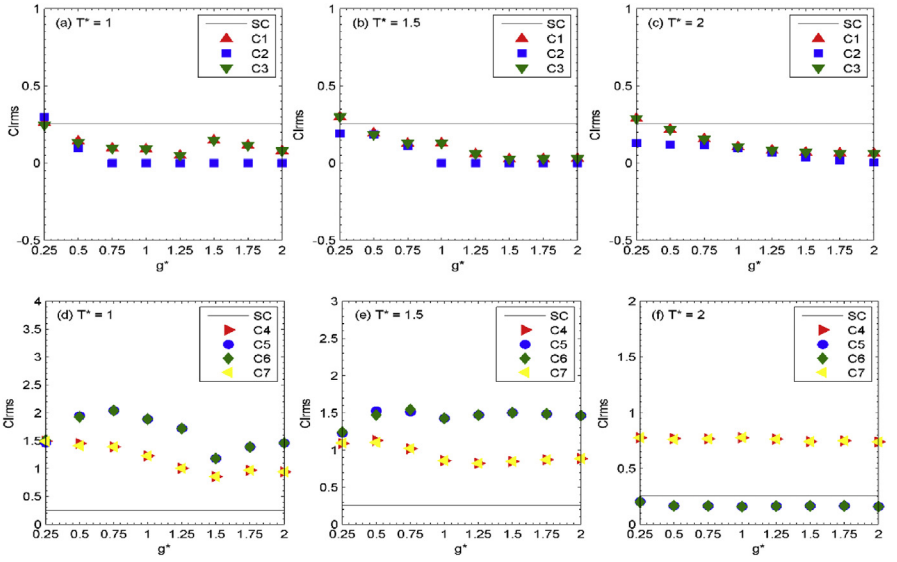

Fig. 16. Variation of root-mean-square value of lift coefficient by varying the values of g* for different fixed T* values (a, d) T* = 1, (b, e) T* = 1.5 and (c, f) T* = 2.

single square cylinder. The maximum and minimum values of Clrms are observed at different position of g* at T* = 1, 1.5 and 2 clearly seen in Fig. 16(a−f). This confirms that the vortex shedding mechanism behind the downstream row of cylinders changes with respect to g* for fixed T* value. Also, (C4, C7) and (C5, C6) show a same behavior in Cdrms for all T* and g* due to symmetricity.

https://doi.org/10.1016/j.heliyon.2019.e01224

5. Conclusion

The numerical studies of flow past two staggered rows of square cylinders at Re = 150 for different fixed value of T* = 1, 1.5 and 2 by varying the gap spacing between the cylinders in streamwise direction from 0.25 to 2 have been performed. The simulations were established based on the single relaxation time lattice Boltzmann method. The studies focus on the changes in the wake structure mechanism behind the downstream row of cylinders and its corresponding hydrodynamic forces. The flow characteristics discussed in this study are seems to be consistent with that mentioned in the literature for side-by-side rows of circular and square cylinders and flow past row of staggered rows of circular cylinders; their placement with respect to gap spacing is, however, different. The difference is due to geometry, numerical scheme and computational domain in the flow. The present computation leads to the following conclusions:

(i) For large streamwise gap spacings ($g^* \geq 1$), fully developed vortex shedding flow is found to characterize the flow field. The shed vortices are clearly visible at the downstream of the computational domain for all T* values. The primary vortex shedding frequency is observed for such kinds of flow structure mechanism.

(ii) Some in-phase/antiphase non-synchronized vortex shedding's are observed for $T^* = 1.5$ and $g^* \geq 1$and the shed vortices behind the downstream row of cylinders are not clearly visible after $x/d \approx 6$.

(iii) The flip-flopping vortex shedding mechanism is observed for small streamwise gap spacings $g^* = 0.25$ to 1 for $T^* = 1$. As a result the vortex shedding behavior behind downstream row of cylinders is strongly affected. The secondary cylinder interaction frequency is the main property of flip-flopping vortex shedding mechanism.

(iv) The mean drag coefficient decreases with increasing streamwise gap spacing. The Strouhal number show some wha constant behavior with little fluctuations. The root-mean-square values of the drag and lift coefficients increases or decreases with increasing streamwise gap spacings.

(v) We found that the vortices generated from the upstream row of cylinders enters through the gap between downstream row of cylinders and is traced behind the downstream row of cylinders for all chosen cases.

(vi) We also found that for $T^* = 1$ at $g^* = 0.25$, 0.5 and 0.75 at small downstream distance ($x/d \approx 2$) behind the downstream row of cylinders the vortices coalesce together and as a result some of the wakes appear wider and narrower as compared to wake behind single square cylinder.

(vii) We also observed symmetric behavior of force statistics and Strouhal number between the downstream row of cylinders across the centre line of

https://doi.org/10.1016/j.heliyon.2019.e01224

computational domain. This phenomenon is not valid for upstream row of cylinders because this row directly faces the incoming flow and due to downstream row of cylinder it does not get the chance to have fully develop vortices even at large T* and g*.

Finally, it is important to state here that the present numerical study is based on two-dimensional computation and the flip-flopping behavior is observed for smaller streamwise gap spacing ($g^* = 0.5$ and 1) may lead to three-dimensionality which can be further numerically investigated through three-dimensional lattice Boltzmann simulation.

Declarations

Author contribution statement

Ghazala Nazeer: Performed the experiments; Wrote the paper.

Shams-ul-Islam: Conceived and designed the experiments; Analyzed and interpreted the data.

Sehrish H. Shigri: Contributed reagents, materials, analysis tools or data.

Funding statement

This research did not receive any specific grant from funding agencies in the public, commercial, or not-for-profit sectors.

Competing interest statement

The authors declare no conflict of interest.

Additional information

No additional information is available for this paper.

References

[1] M.M. Zdravkovich, Review of flow interference between two circular cylinders in various arrangements, ASME J. Fluids Eng. 99 (1977) 618−633.

[2] S. Kang, Characteristics of flow over two circular cylinders in a side-by-side arrangement at low Reynolds numbers, Phys. Fluid. 15 (2003) 2486−2498.

[3] S. Kang, Numerical study on laminar flow over three side-by-side cylinders, KSME Int. J. 18 (2004) 1869−1879.

https://doi.org/10.1016/j.heliyon.2019.e01224

[4] M.M. Alam, Y. Zhou, X.W. Wang, The wake of two side-by-side square cylinders, J. Fluid Mech. 669 (2011) 432−471.

[5] D.W. Guillaume, J.C. LaRue, Investigation of the flopping regime with three- and four-cylinder arrays, Exp. Fluid. 27 (1999) 145−156.

[6] H.K. Virahsawmy, L. Chen, I.R. MacGillivray, J. Tu, Y. Zhou, Computation of flow behind three side-by-side cylinders of unequal/equal spacing, ANZIAM J. 46 (2005) C672−C989.

[7] W. Wang, H.J. Zhang, Y. Zhou, J.Y. Tu, Flow visualization behind three cylinders of equal and unequal spacing, Int. J. Flow Visu. Image Proc. 9 (2002) 139−151.

[8] H.J. Zhang, Y. Zhou, Effect of unequal cylinder spacing on vortex streets behind three side-by-side cylinders, Phys. Fluid. 13 (2001) 3675−3686.

[9] H. Zhaolong, D. Zhou, J. Tu, Laminar flow patterns around three side-by-side arranged circular cylinders using semi-implicit three-step Taylor-characteristic-based-split (3-TCBS) algorithm, Eng. App. Comp. Fluid Mech. 7 (2013) 1−12 (2013).

[10] J. Mizushima, Y. Takemoto, Stability of the flow past a row of square bars, J. Phys. Soc. Japan. 65 (1996) 1673−1685.

[11] A. Agrawal, L. Djendi, R.A. Antonia, Investigation of flow around of a pair of side-by-side square cylinders using the lattice Boltzmann method, Comput. Fluid. 35 (2006) 1093−1107.

[12] O. Inoue, W. Iwakami, N. Hatakeyama, Aeolian tones radiated from flow past two square cylinders in a side-by-side arrangement, Phys. Fluid. 18 (046104) (2006) 1−20.

[13] O. Inoue, Y. Suzuki, Beat of sound generated by flow past three side-by-side square cylinders, Phys. Fluid. 19 (048102) (2007) 1−4.

[14] W.S. Abbasi, S. Ul. Islam, S.C. Saha, Y.T. Gu, C.Y. Zhou, Effect of Reynolds numbers on flow past four square cylinders in an in-line square configuration for different gap spacings, J. Mech. Sci. Technol. 28 (2014) 539−552.

[15] S. Ul. Islam, H. Rahman, C.Y. Zhou, S.C. Saha, Comparison of wake structures and force measurements behind three side-by-side cylinders, J. Braz. Soc. Mech. Sci. Eng. 38 (2016) 843−858.

[16] H. Rahman, S. Ul. Islam, C.Y. Zhou, T. Kiyani, S.C. Saha, On the effect of Reynolds number for flow past three side-by-side square cylinders for unequal gap spacings, KSCE J. Civil Eng. 19 (2015) 233−247.

https://doi.org/10.1016/j.heliyon.2019.e01224

[17] S.C. Yen, C.T. Liu, Gap-flow patterns behind twin-cylinders at low Reynolds number, J. Mech. Sci. Technol. 25 (2011) 2795–2803.

[18] J. Mizushima, T. Akinaga, Vortex shedding from a row of square bars, Fluid Dyn. Res. 32 (2003) 179–191.

[19] L. Djenidi, Lattice Boltzmann simulation of grid-generated turbulence, J. Fluid Mech. 552 (2006) 13–35.

[20] S.R. Kumar, A. Sharma, A. Agrawal, Simulation of flow around a row of square cylinders, J. Fluid Mech. 606 (2008) 369–397.

[21] C.M. Sewatkar, A. Sharma, A. Agrawal, On the effect of Reynolds number for flow around a row of square cylinders, Phys. Fluid. 21 (2009), 083602(1–13).

[22] H.J. Kim, P.A. Durbin, Investigation of the flow between a pair of circular cylinders in the flopping regime, J. Fluid Mech. 196 (1988) 431–448.

[23] M.P. Chauve, P. Le Gal, Complex bi-orthogonal decomposition of chain of coupled wakes, Phys. D. 58 (1992) 407–413.

[24] D. Chatterjee, G. Biswas, Dynamic behavior of flow around rows of square cylinders kept in staggered arrangement, J. Wind Eng. Ind. Aerod. 136 (2015) 1–11.

[25] M.M. Zdravkovich, K.L. Stonebanks, Intrinsically nonuniform and metastable flow in and behind tube arrays, J. Fluid Struct. 4 (1990) 305–319.

[26] A.V. de Paula, S.V.M. Moller, State space reconstruction of experimental time series of bistable flow on a tube bank, in: C. Meskell, C. Bennett (Eds.), Proceedings of the 10th International Conference on Flow-Induced Vibration, Dublin, Ireland, 2012, pp. 499–506.

[27] P. Anagnostopoulos, S.A. Seitanis, Numerical study of aperiodic phenomena past two staggered rows of cylinders in cross-flow, Ocean Eng. 92 (2014) 212–233.

[28] M. Junk, A. Klar, L.-S. Luo, Asymptotic analysis of the lattice Boltzmann equation, J. Comp. Phys. 210 (2005) 676–704.

[29] Z. Guo, C. Shu, Lattice Boltzmann method and its applications in engineering (advances in computational fluid dynamics), World Sci. Pub. Comp. (2013). https://books.google.com.pk/books?id=-Zy6CgAAQBAJ.

[30] P.L. Bhatnagar, E.P. Gross, M. Krook, A model for collision processes in gases. I. Small amplitude processes in charged and neutral one-component systems, Phys. Rev. 94 (1954) 511–525.

https://doi.org/10.1016/j.heliyon.2019.e01224

[31] Z. Guo, H. Liu, L.-S. Luo, K. Xu, A comparative study of the LBE and GKS methods for 2D near incompressible laminar flows, J. Comp. Phys. 27 (2008) 4955−4976.

[32] M.C. Sukop, D.T. Thorne Jr., Lattice Boltzmann Modeling: an Introduction for Geoscientists and Engineers, Springer-Verlag Berlin Heidelberg, 2006 & 2007.

[33] Y. Chen, Q. Cai, Z. Xia, M. Wang, S. Chen, Momentum-exchanged method in lattice Boltzmann simulations of particle-fluid interactions, Phys. Rev. E. 88 (1−15) (2013), 013303.

[34] D. Yu, R. Mei, L.-S. Luo, W. Shyy, Viscous flow computations with the method of lattice Boltzmann equation, Prog. Aero. Sci. 39 (2003) 329−367.

[35] B. Gera, P.K. Sharma, R.K. Singh, CFD analysis of 2D unsteady flow around a square cylinder, Int. J. App. Eng. Res. Dindigual 1 (2010) 602−610.

[36] A. Sohankar, C. Norberg, L. Davidson, Numerical simulation of unsteady Low-Reynolds number flow around rectangular cylinders at incidence, J. Wind Eng. Ind. Aerod. 69 (1997) 189−201.

[37] Y. Wang, C. Shu, C.J. Teo, J. Wu, An immersed boundary-lattice Boltzmann flux solver and its applications to fluid−structure interaction problems, J. Fluid Struct. 54 (2015) 440−465.

[38] M. Cheng, P.M. Moretti, Experimental study of the flow field downstream of a single tube row, Exp. Therm. Fluid Sci. 1 (1988) 69−74.

https://doi.org/10.1016/j.heliyon.2019.e01224